Experimental investigation and modeling of the spread and burning behaviors of continuous spill fires on a water surface

Jinlong Zhao, Guangheng Song, Xiang Zhang, Yuntao Li, Jianping Zhang, Rui Yang

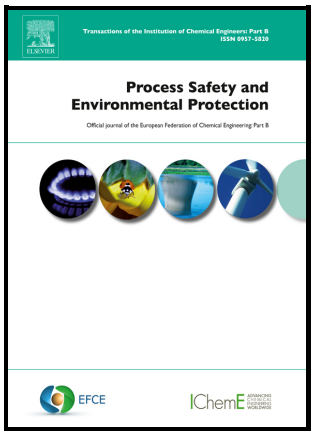

PII: S0957-5820(22)00845-X

DOI: https://doi.org/10.1016/j.psep.2022.09.071

Reference: PSEP3928

To appear in: *Process Safety and Environmental Protection*

Received date: 11 May 2022
Revised date: 25 July 2022
Accepted date: 27 September 2022

Please cite this article as: Jinlong Zhao, Guangheng Song, Xiang Zhang, Yuntao Li, Jianping Zhang and Rui Yang, Experimental investigation and modeling of the spread and burning behaviors of continuous spill fires on a water surface, *Process Safety and Environmental Protection,* (2022) doi:https://doi.org/10.1016/j.psep.2022.09.071

Experimental investigation and modeling of the spread and burning behaviors of continuous spill fires on a water surface

Jinlong Zhao[a], Guangheng Song[a], Xiang Zhang[a], Yuntao Li[b], Jianping Zhang[c*], Rui Yang[d]

[a]*School of Emergency Management & Safety Engineering, China University of Mining & Technology, Beijing 100083, China*

[b]*College of Safety and Ocean Engineering, China University of Petroleum, Beijing 102299, China*

[c]*FireSERT, Belfast School of Architecture and the Built Environment, Ulster University, Newtownabbey, BT37 0QB, United Kingdom*

[d]*Institute of Public Safety Research, Department of Engineering Physics, Tsinghua University, Beijing 100084, China*

The corresponding author: Jianping Zhang

FireSERT, Belfast School of Architecture and the Built Environment

Ulster University, Newtownabbey, United Kingdom

E-mail: j.zhang@ulster.ac.uk

Tel: +44 2890366460

Abstract: Spill fires caused by oil leakage from tankers may pose a threat to the liquid transportation safety. In this paper, a series of large-scale gasoline continuous spill fire experiments were conducted on a water surface. The spread area, flame height, burning rate and the temperatures in the water layer were measured for different fuel discharge rates and ignition delays. The findings show that the spread process can be well predicted by an existing spread model without ignition. For ignited conditions, four burning phases were identified, namely (i) spread burning phase, (ii) shrinking burning phase, (iii) quasi-steady burning phase, and (iv) extinguishment phase. The burning rate at the quasi-steady phase was found to be approximately 45 to 62 % that of pool fires with the same burning area. Subsequently, a model was developed for predicting the quasi-steady burning rate of spill fires. The flame height at the quasi-steady burning phase was also analyzed and correlated with the fuel discharge rate. Finally, a model was proposed to predict the maximum burning area at the spread burning phase and validated against the experimental data. The present results are of practical importance in understanding of the spread and burning characteristics of

continuous spill fires and the associated risk assessment.

Keywords: continuous spill fire, fuel spread, burning rate, maximum burning area, spread model

1. Introduction

The global demand of liquid fuels is ever increasing driven by the fast development of the world economy. Marine transportation using oil tankers plays an important role in the transportation of liquid petroleum products due to its low cost (Soares da Silva et al., 2021). One of the potential risks during the transportation process is the leakage of the fuel on the water surface. Once the liquid fuel leaks, it is often followed by ignition and subsequently the occurrence of a spill fire, which poses a greater threat to the safety of the people on board, the fuel transported, and the marine enviroment (Palazzi et al., 2004; Raja et al., 2019). Compared with a pool fire, the burning area of a spill fire is unconfined because there is no horizontal boundary, which means a larger burning area and a higher thermal risk (Zhao et al., 2017). For example, in 2018, a spill fire accident occurred after the collision of the oil tanker Sanchi at East China Sea and the leakage of the fuel resulted in a total burning area of approximately 70,000 m^2 and the death of 32 crew members (Yin et al., 2021). It is therefore of great importance to study the spread and burning behaviors of spill fires in order to understand better the fire risk associated with the marine transportation of liquid fuels .

The fire risk during the transportation process of liquid fuels is closely related to the spread and burning processes (Palazzi et al., 2004; Bonvicini et al., 2015). For the spread of liquid fuels, Fay (1969) conducted experiments of fuel spread on a water surface and analyzed the spread process for different discharge rates and found that, based on order-of-magnitude analysis, the spread process can be distinguished into three regimes: ‘gravity-inertia’ regime, ‘gravity-viscous’ regime and ‘surface tension-viscous’ regime. Briscoe and Shaw (1980) studied the spread of liquid fuels on a water surface and noted that the spread process was mainly controlled by gravity and the inertial force, based on which a spread model was developed and subsequently used by other researchers (Raj, 2011; Webber, 2012). These studies laid a foundation for the research on the spread and burning processes of liquid fuels. For the burning of spill fires, the burning rate developed for pool fires is sometimes used to calculate the liquid fuel consumption during the spread process (Fay, 2003; Lehr and Simecek-Beatty, 2004). However, studies have shown that this simplification could result in large discrepancies in the calculations. Gottuk et al. (2000) conducted spill fire experiments

on a concrete surface and found that the burning rate of spill fires was around 20 % of that in pool fires for the same burning area. Mealy et al. (2014) conducted spill fire experiments on different substrates (concrete, vinyl and plywood) and found that the heat loss of the thin fuel layer to the substrates is a key factor contributing to the lower burning rate in spill fires.

In recent years, the spread and burning processes of continuous spill fire experiments were examined by several research groups (Li et al., 2017; Ingason and Li, 2017; Zhao et al., 2019; Pan et al., 2020; Li et al., 2020). Li et al. (2017) performed continuous spill fire experiments in a steel trench (3 m × 0.15 m) and divided the whole spread process into five phases (spread, shrinking process, quasi-steady burning, maintenance after discharge time and fire extinction). Ingason and Li (2017) conducted continuous spill fires on a concrete surface with different slopes and found that the larger slope the concrete surface, the smaller the heat release rate. In Zhao et al. (2019), the authors carried out continuous spill fire experiments on a fireproof glass surface and the heat transfer between the fuel layer and glass was studied, based on which a model incorporating the heat loss of the fuel layer was developed. Pan et al. (2020) carried out continuous spill fire experiments on a rectangular steel trench (1 m × 0.044 m) and reported that the discharge rate also affected the burning rate. Li et al. (2020) conducted continuous spill fires in a model-scale tunnel and qualitatively analyzed the heat transfer process of the fuel layer, in which the spill fire burning rate was revised using an empirical correction factor provided by Mealy et al. (2014). These studies have qualitatively clarified some of the key factors affecting the burning rate and further verified that the heat loss of the fuel layer plays an important role in the reduced burning rate of continuous spill fires. However, in these studies, the heat loss from the fuel layer to the substrate and the maximum burning area (one of the key parameters to assess the risk of spill fire accidents) were not examined in detail.

In this work, large-scale continuous spill fires experiments were carried out on a water surface. The spread and burning behaviors were recorded for different fuel discharge rates and ignition delays. The temperature profile in the water layer was measured to quantify the heat loss of the fuel layer to the water layer, based on which a numerical model was developed to predict the burning rate of spill fires. By combining the fuel spread model and the burning rate model, the maximum burning area was calculated and validated against the experimental data. These results are important in assessing the risks in a spill fire accident during marine transportation and conducting

in-situ burning which can be used to reduce the adverse effect of the leaked fuel on the environment.

2. Experimental setup

The experimental schematic is shown in Fig. 1(a). The stainless circular pan has an inner diameter of 6 m, which is sufficient to minimize the boundary effect on the fuel spread. The height of the side wall is 0.3 m. Before the experiments, the pan was filled with water of 25 cm, which was found to be sufficiently deep that the heat does not penetrate the water layer and its effect on burning can be neglected (Garo et al., 1999). During the experiments, the fuel (92# gasoline) was discharged from the outlet positioned at the center of the pan to spread on the water surface. The detail position is shown in Fig. 1. Preliminary tests were conducted to adjust the angle of the discharge outlet, so that the fuel can spread in an axisymmetric manor. A peristaltic pump was used to provide a steady volumetric flow rate ranging from 0.06 to 18 mL/s. A Sartorius balance (maximum load: 35 kg, accuracy: 0.1 g) was used to record the residual mass and to ensure the desired discharge rate Q_{in}. Five thermocouple trees were placed outward from the center of the pan at 10 cm intervals. Each thermocouple tree consisted of five K-type thermocouples (tip of 0.5 mm, resolution ±1 K) located on the water surface and at 0.5, 1, 2 and 3 cm below as shown in Fig. 1(c). Two digital video (DV) recorders (SONY HDR-CX450) were used to record the spread process, based on which the real-time spread area and flame height were determined. DV 1 was located at an elevated location with the lens tilted at an angle, so that the front of the fuel layer can be captured clearly. DV 2 was located at 15 m away to record the flame height.

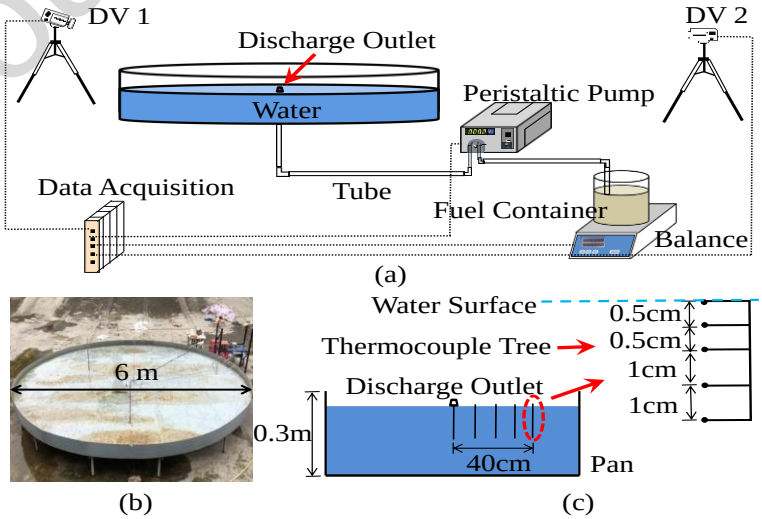

Fig. 1. Schematic diagram of: a) complete experimental set-up; b) the stainless pan; c) thermocouples arrangement in the water layer.

All tests were conducted outdoors, and the wind velocity was less than 0.2 m/s, so the effect of the wind could be ignored. The ambient temperature was 24±3 ℃. In total, 20 test configurations were considered with different fuel discharge rates and ignition delays (the time delay in igniting the fuel after the initial release) as shown in Table 1. The discharge duration was chosen to allow the establishment of the quasi-steady steady burning stage for the determination of the corresponding burning area. Each test configuration was repeated twice, and the results showed good repeatability. The relative errors were less than 11.6％for the measured quasi-steady diameters.

Table 1 Specification of the test conditions.

Test No.	Discharge rate, Q_{in} (mL/s)	Ignition delay, t_s (s)	Discharge duration (s)	Total volume (mL)
1	3.0	No ignition	320	960
2	6.0	No ignition	270	1620
3	9.0	No ignition	240	2160
4	14.0	No ignition	150	2100
5	3.0	0	147	441
6	6.0	0	140	840
7	9.0	0	126	1134
8	14.0	0	154	2156
9	3.0	10	190	570
10	6.0	10	190	1140
11	9.0	10	190	1710
12	14.0	10	190	2660
13	3.0	20	200	600
14	6.0	20	200	1200
15	9.0	20	200	1800
16	14.0	20	200	2800
17	3.0	30	210	630
18	6.0	30	210	1260
19	9.0	30	210	1890
20	14.0	30	210	2940

3. Results and discussion

3.1 Spread process of liquid fuel

3.1.1 Spread process without ignition

For a liquid fuel spreading on a water surface, the ‘gravity-inertia’ regime has been shown to play a dominant role in the spread area (Briscoe and Shaw, 1980; Lehr and Simecek-Beatty, 2004). In this regime, Briscoe and Shaw (1980) developed a spread

model based on the balance of gravity and the inertial force, which was widely used to predict the fuel spread process (e.g., Raj, 2011; Webber, 2012):

$$\frac{dR}{dt} = \varepsilon\sqrt{g'h} \tag{1}$$

where R is the spread radius (m), t is the spread time (s), h is the average fuel layer thickness (m), $g'$is the effective gravity that is a function of the density of fuel and water ($g' = g\left(1\text{-}\rho_f/\rho_w\right)$), and ε is an empirical constant and its value is usually determined by experimental data.

The average fuel layer thickness h can be calculated as the ratio between the discharge volume and the fuel spread area. Therefore, Eq. (1) becomes:

$$\frac{dR}{dt} = \varepsilon\sqrt{g'\frac{Q_{in}t}{\pi R^2}} \tag{2}$$

where Q_{in} is the fuel discharge rate (mL/s). By integrating Eq. (2), one obtains:

$$R = \left[\frac{4}{3}\varepsilon\left(\frac{1}{\pi}\right)^{1/2}\right]^{1/2}(g'Q_{in})^{1/4}t^{3/4} \tag{3}$$

Eq. (3) indicates that the spread radius, R, is proportional to $(g'Q_{in})^{1/4}t^{3/4}$. By plotting R against $(g'Q_{in})^{1/4}t^{3/4}$, the spread coefficient, ε, can be determined, as shown in Fig. 2.

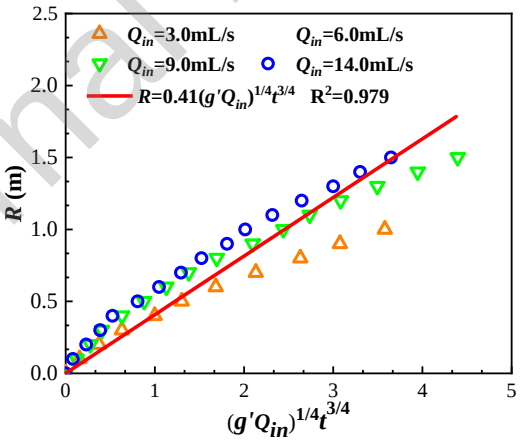

Fig. 2. The spread radius as a function of $(g'Q_{in})^{1/4}t^{3/4}$ for different fuel discharge rates.

As shown in Fig. 2, the spread coefficient was found as $\varepsilon\approx0.23$. Note that there is a relatively large difference between the experimental data and the correlation for larger values of $(g'Q_{in})^{1/4}t^{3/4}$, which could be attributed to the fact that the fuel spread regime is gradually changing from the 'gravity-inertia' to the 'gravity-viscous' regime. Another possible reason is that at longer times the shape of the spread fuel could not kept completely axisymmetric, for which case the average spread radius was estimated.

3.1.2 Spread process with ignition

To display the whole burning spread process, typical flame images for Test 8 (Q_{in} =14.0 mL/s and with no ignition delay, i.e., t_s=0) are shown in Fig. 3.

Fig. 3. Images of continuous spill fire at different times after discharge in Test 8.

It can be seen in Fig. 3 that from 10 to 40 s, both the flame diameter and flame height increased rapidly. However, the flame diameter decreased from 95 cm at 40 s to 79 cm at 90 s. During this period, the fuel burning rate ($\omega\pi R^2$, where ω is the linear burning rate, m/s) gradually increased and became larger than the discharge rate ($\omega\pi R^2 >$14.0 mL/s), and, as a result, there was no fresh fuel to be fed to the fuel front, which led to the shrink of the burning area. From 90 to 142 s, the burning area and flame height remained nearly constant, indicating a balance between the fuel burning rate and the discharge rate. After the fuel supply was stopped, both the burning area and flame height decreased gradually before the fire eventually extinguished.

These spread behaviors were also observed in other tests and the detail spread process is shown in Fig. 4, which shows the variation of the spread radius as a function of time at different discharge rates with no ignition delay.

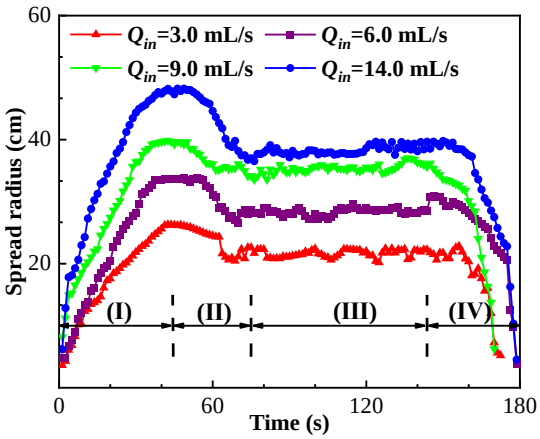

Fig. 4. The spread radius as a function of time for different discharge rates (No ignition delay).

The spread process, as shown in Fig. 4, can be divided into four phases: (i) spread

burning phase, (ii) shrinking burning phase, (iii) quasi-steady burning phase, and (iv) extinguishment phase, which correspond well with those reported by Li et al. (2021a). Fig. 5 shows the variation of both the quasi-steady burning area and the maximum burning area at different discharge rates and ignition delays.

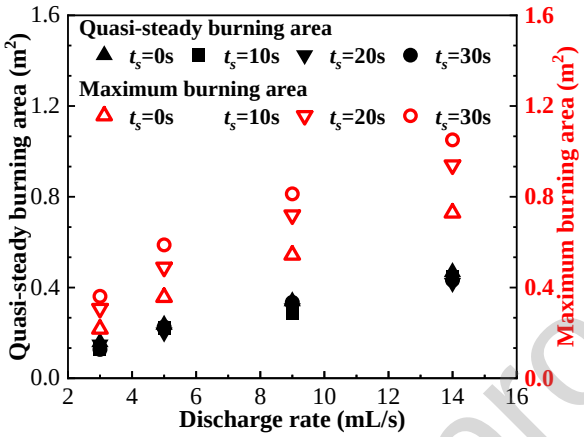

Fig. 5. The quasi-steady burning area and maximum spread area for different discharge rates and ignition delays (t_s).

As shown in Fig. 5, the quasi-steady burning area is independent of the ignition delay but increases with the discharge rate. This is because the fuel burning rate at this phase was approximately the same as the fuel discharge rate. The maximum burning area, on the other hand, increases with the ignition delay. For example, the maximum burning area for the case with Q_{in}= 14.0 mL/s and t_s=30 s was 1.05 m^2, which is 43.8% larger than that (0.73 m^2) for the test at the same discharge rate but with no ignition delay. In order to further examine the effect of the ignition delay, a ratio φ can be defined as:

$$\varphi=\frac{A_m-A_0}{A_0}\times 100\% \quad (4)$$

where A_m is the maximum burning area at a given ignition delay (t_s=0, 10, 20, or 30 s) (m^2), and A_0 is the maximum burning area for instantaneous ignition (t_s = 0 s) (m^2). Fig. 6 shows the ratio φ increases almost linearly with the ignition delay.

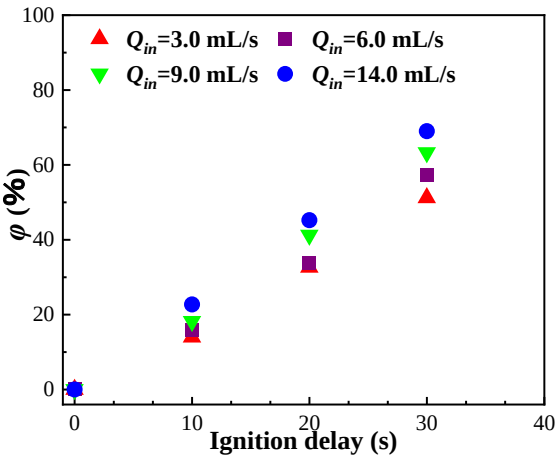

Fig. 6. The ratio φ as a function of ignition delay at different discharge rates.

It is worth noting that if the release was continuous (with no ignition) and the evaporation, viscosity and surface tension effects are not considered, the ratio φ would continuously increase with the ignition delay. In practical situations, the increase of the ratio φ will be limited due to the balance between evaporation and discharge rate. For the liquid spread with no ignition, as the fuel surface increases, the spread rate will gradually decrease due to the weak gravity effect, whereas evaporation will become more important. It can also be observed in Fig. 6 that for the same ignition delay, the ratio φ increases with the discharge rate, since at a larger discharge rate the fuel can spread to a larger area before ignition.

3.2 Quasi-steady burning behaviors

3.2.1. Burning rate of spill fires

During the quasi-steady burning phase, the fuel burning rate ($\pi\omega_s R_s^2$) is dynamically balanced by the fuel discharge rate (Q_{in}):

$$\omega_s = \frac{Q_{in}}{\pi R_s^2} \tag{5}$$

where ω_s is the linear burning rate in the quasi- steady burning phase (m/s).

Babrauskas (1983) proposed an empirical relationship between the burning rate and burning diameter for pool fires:

$$\omega_{pool} = \omega_\infty\left(1 - e^{-k\beta D}\right) \tag{6}$$

where ω_∞ is the linear burning rate of a pool fire with an infinite diameter (m/s), k is the flame extinction coefficient (1/m), β is the mean-beam length corrector, and D is the pool diameter (m). Fig. 7 shows a comparison of the experimental burning rates and those predicted by the pool fire model using Eq. (6).

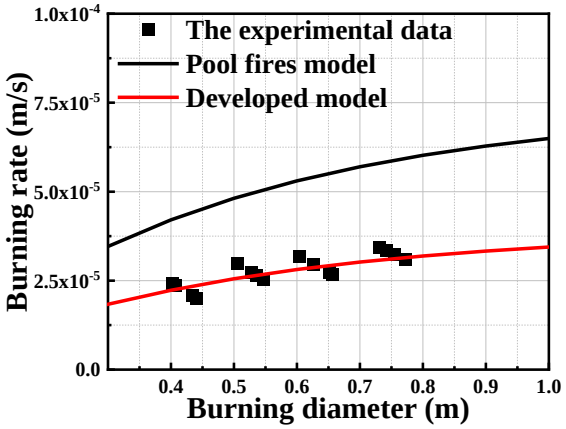

Fig. 7. Comparison of experimental burning rate with that predicted by the model for pool fires and the present one developed for spill fires.

Fig. 7 shows that the burning rate of spill fires gradually increases with the burning diameter, similar to that observed for pool fires. This can be explained by noting that for a large burning area (D > 0.2 m), the radiative heat feedback from the flame to the fuel surface is the dominant heat transfer mechanism controlling the burning rate (Hamins et al., 1994). The radiative heat feedback can be expressed as (Ditch et al., 2013):

$$q_{rad} = \sigma\left(T_{rf}^4 - T_0^4\right)[1 - exp(-\kappa D)] \quad (7)$$

where σ is the Stefan–Boltzmann constant, T_{rf} is an effective flame radiation temperature (K), T_0 is the ambient temperature (K), and κ is an effective absorption–emission coefficient. As the burning diameter increases, the radiative heat feedback increases, leading to an increase of the burning rate.

The experimental burning rates of spill fires are systematically lower than those predicted by the model for pool fires – about 45 to 62 % of the predicted values. In order to explain this, it is important to examine the difference in the heat transfer process between pool fires and spill fires as illustrated in Fig. 8.

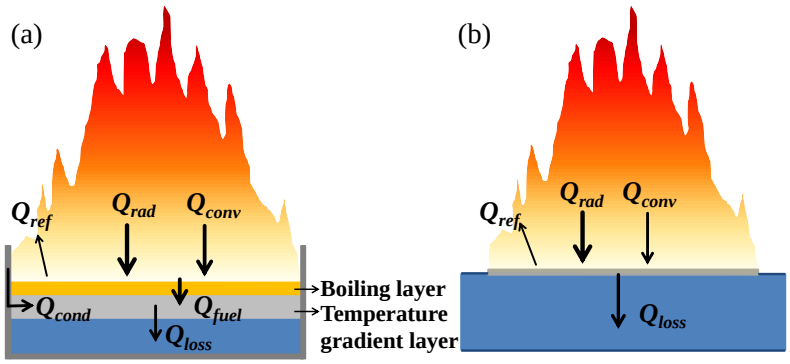

Fig. 8. Heat transfer in the fuel layer for (a) a pool fire and (b) a spill fire.

In pool fires, the heat transfer process can be expressed as (Hamins et al., 1994):

$$Q_{cond} + Q_{conv} + Q_{rad} = Q_{fuel} + Q_{loss} + Q_{ref} \quad (8)$$

where Q_{cond}, Q_{conv} and Q_{rad} are, respectively, conduction from the side wall, convection due to combustion gas, and radiation from the flame (kJ). Q_{fuel} represents the heat absorbed by the fuel. Q_{loss} is the heat loss of the fuel layer to the bottom of the fuel pan, which can usually be neglected for pool fires because the heat is completely absorbed by the thick liquid layer (Suo-Anttila et al., 2009; Zhao et al., 2020). The reflected heat Q_{ref} is typically small compared to other terms and is therefore neglected (Hamins et al., 1994).

Since the quasi-steady burning diameter in our experiments is more than 0.3 m, Q_{rad} is dominant in controlling the burning rate (Hamins et al., 1994). Eq. (8) can be simplified to (Vali et al., 2015):

$$q_{rad} = \omega_{pool}\rho_f(\Delta H_v + c_{pf}(T_b - T_0) \quad (9)$$

where ΔH_v is the latent heat of evaporation (kJ/kg), T_b is the liquid fuel boiling point (K) and T_0 is the ambient temperature (K), and c_{pf} is the average specific heat of the fuel from T_0 to T_b (kJ/kg-K).

The radiative heat feedback for spill fires can be calculated similarly but with the burning rate for spill fires. In contrast to pool fires, the heat transfer process between the fuel layer and the water layer in spill fires is significant and should be considered (Garo et al., 1999), because the fuel thickness is in the order of millimeters (Maly et al., 2014). This is evident in Fig. 9 showing the temperature histories at different depths in the water layer (Test-8, at 20 cm to the discharge outlet).

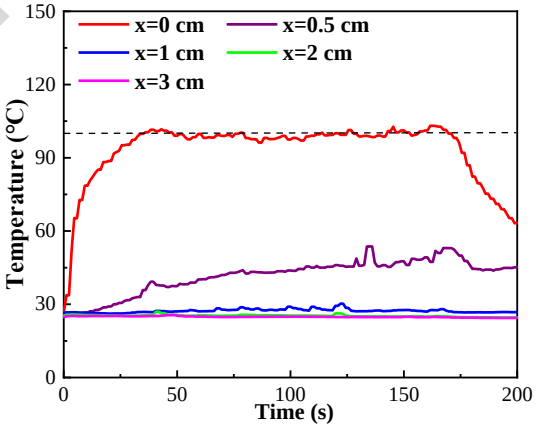

Fig. 9. The measured temperature by the thermocouple tree positioned at 20 cm to the discharge outlet in Test-8.

Figure 9 shows that the temperature at the water surface increases quickly after the initial contact with the fuel layer, followed by a nearly constant value close to the

boiling point of the fuel, which indicates that the temperature inside the fuel layer is nearly uniform. However, the temperature at 1 cm or deeper remains nearly at the ambient temperature. Based on the temperature variations in the water layer, the heat loss at a distance, *x*, to the outlet can be found as (Vali et al., 2015):

$$q'_{lossx} = c_{pw}\rho_w \int_0^{h_0} \frac{dT}{dt} dh \tag{10}$$

where c_{pw} is the specific heat capacity of water (kJ/kg-K), h_0 is the thickness of the heat penetration depth in the water layer (m), and *T* is the water temperature (K). Table 2 presents the calculated results of the average heat loss values based on the measured water temperatures. The heat loss near the discharge outlet is lower than that at other positions because of the supply of the fresh fuel. With an increase in the distance from the outlet, the heat loss gradually increases before reaching a constant value, which could be attributed to the steady fuel temperature (around the boiling point) after the initial heating phase.

Table 2 The calculative heat flux loss values (unit: kW/m^2).

Distance from discharge outlet (cm)	Q_{in}=3.08 mL/s	Q_{in}=5.97 mL/s	Q_{in}=9.08 mL/s	Q_{in}=14.44 mL/s
0	6.16	7.41	7.16	8.18
10	9.82	11.54	11.81	14.17
20	12.36	12.23	14.82	15.54
30	12.56	14.62	15.16	15.38
40	13.85	15.07	15.57	15.86

Based on the heat losses at different locations, the average heat loss can be found as:

$$q'_{loss} = \frac{\sum_{i=1}^{n}(\pi x_i^2 - \pi x_{i-1}^2) q'_{lossx(i-1)}}{\pi R^2} \tag{11}$$

where *i* the number of a given thermocouple tree, *n* is the total number of thermocouple trees, x_i is the distance to the discharge outlet. $(\pi x_i^2 - \pi x_{i-1}^2)$ is the area of the circular ring. $q'_{lossx(i-1)}$ is the heat loss at the position of the $(i\text{-}1)^{th}$ thermocouple tree. Therefore, the burning rate of spill fires at the quasi-steady burning phase can be expressed as:

$$q_{rad} - q'_{loss} = \omega_{spill}\rho_f(\Delta H_v + c_p(T_b - T_0)) \tag{12}$$

Based on Eqs. (8-12), the quasi-steady burning rate of continuous spill fires can be deduced as:

$$\omega_{spill} = \left(1 - q'_{loss}/q_{rad}\right)\omega_{pool} \tag{13}$$

or

$$\omega_{spill} = C_\delta \omega_\infty \left(1 - e^{-k\beta D}\right) \tag{14}$$

where C_δ=$\left(1\text{-}\, q'_{loss}/q_{rad}\right)$. The predicted values by Eq. (14) are shown in Fig. 7, in close agreement with the measured values. These results further verify that the increased heat loss of the fuel layer is the primary reason for the reduced burning rate in spill fires.

3.2.2 Flame height

For the prediction of the flame height, (Heskestad, 1999) proposed a dimensionless correlation:

$$H/D = 3.7\left(\dot{Q}^*\right)^{2/5} - 1.02 \tag{15}$$

where D is the diameter of the fire (m), and $\dot{Q}^*$ is the dimensionless heat release rate:

$$\dot{Q}^* = \frac{\dot{Q}}{\rho_\infty c_{pa} T_\infty g^{1/2} D^{5/2}} \tag{16}$$

where ρ_∞ is the ambient density (kg/m^3), T_∞ is the ambient temperature (K), g is the gravity acceleration (=9.81m/s^2) and c_{pa} is the specific heat of air at constant pressure (kJ/kg-k). $\dot{Q}$ is the total heat release rate (kW), which can be calculated from the fuel discharge rate as:

$$\dot{Q}=\rho_f Q_{in} H_c \tag{17}$$

where H_c is the effective heat of combustion (kJ/kg).

Figure 10 shows a comparison of the measured average flame height at the quasi-steady burning stage and that predicted using Eq. (15).

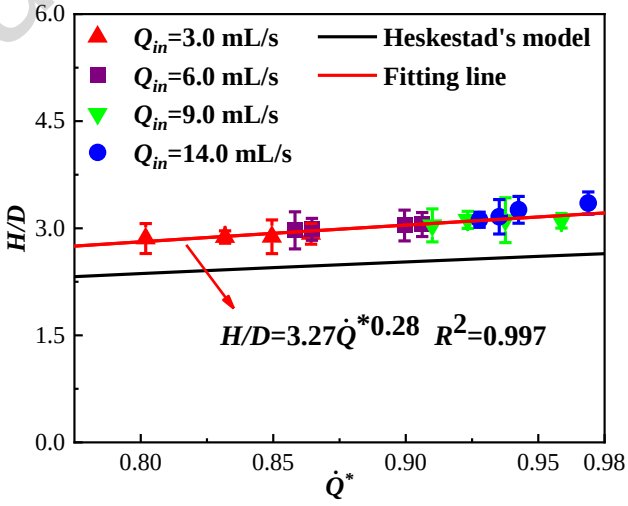

Fig. 10. Comparison of experimental average flame height with that predicted by Heskestad's model.

The predicted values are slightly lower than the experimental data, even though the trends are similar. This can be attributed to that the model was deduced based on pool fires, in which there is a sidewall which could increase air entrainment around the sidewall rim, leading to a lower flame height.

For spill fires, the flame height is related to the discharge rate, diameter of the burning area, heat release rate, and fuel layer thickness, i.e.,

$$H = fcn(Q_{in}, D, \dot{Q}, h) \tag{18}$$

Based on dimensionless analysis, Eq. (18) can be simplified as (Moorhouse, 1982; Zukoski et al., 1985):

$$H/D = a(\dot{Q}^*)^b \tag{19}$$

where *a* and *b* are model constants, and their values can be determined based on experiment data. In this study, the values of *a* and *b* for continuous spill fires are found to be 3.27 and 0.28 respectively as shown in Fig. 10 and Eq. (20).

$$H/D = 3.27(\dot{Q}^*)^{0.28} \tag{20}$$

3.3 Spread and burning model

The burning rate and flame height presented in Section 3.2 are for the quasi-steady stage. In this section, a model is developed to predict the transient spread and burning process and the maximum burning area at the spread burning phase.

For the fuel spread on the water surface, the heat transfer through fuel and water is nearly one-dimensional. The conduction equations for the fuel and water layers can be expressed as (Garo et al., 1999):

$$\rho_f c_{pf} \frac{\partial T}{\partial t} = k_f \frac{\partial^2 T}{\partial x^2} + \frac{\partial q_r}{\partial x} \tag{21}$$

$$\rho_w c_{pw} \frac{\partial T}{\partial t} = k_w \frac{\partial^2 T}{\partial x^2} + \frac{\partial q_r}{\partial x} \tag{22}$$

with the initial condition:

$$t=0,\ T=T_0 \tag{23}$$

where k_f, k_w are the thermal conductivity of fuel and water, respectively (kW/m-K).

Based on the finding of Suo-Anttila et al. (2009), the heat feedback from the flame is mainly absorbed by the upper liquid layer (~3 mm), which results in a thin boiling layer. In our experiments, the fuel layer thickness was less than 1 mm during the whole spread process. Therefore, the fuel layer can be simplified as one with a uniform temperature (boiling point) (Suo-Anttila et al., 2009). The measured temperature (99°C) at the fuel-water interface also validates this simplification, as shown in Fig. 9. As water has strong radiative absorption, the heat transfer process can be further simplified as (Garo

et al., 1999; Brambilla and Manca, 2009):

$$\frac{\partial T}{\partial t} = \alpha_w \frac{\partial^2 T}{\partial x^2} \tag{24}$$

where α_w is the thermal diffusivity of water (m^2/s).

In the calculations, the temperature of the water surface is considered to be the fuel boiling point. The real time temperature distribution in the water layer and the heat loss of the fuel layer can be calculated, respectively, as:

$$\frac{T(x,\ t)-T_s}{T_0-T_s} = erf\left(\frac{x}{2\sqrt{\alpha_w t}}\right) \tag{25}$$

$$q'_{loss}(t) = \frac{k_w(T_s-T_0)}{\sqrt{\pi\alpha_w t}} \tag{26}$$

with the initial condition:

$$T(x, 0) = T_0 \tag{27}$$

In order to verify the accuracy of this method, Fig. 11 shows a comparison of the predicted and measured temperatures. There is a good agreement between the experimental data and predicted values with a maximum difference of 10.3%.

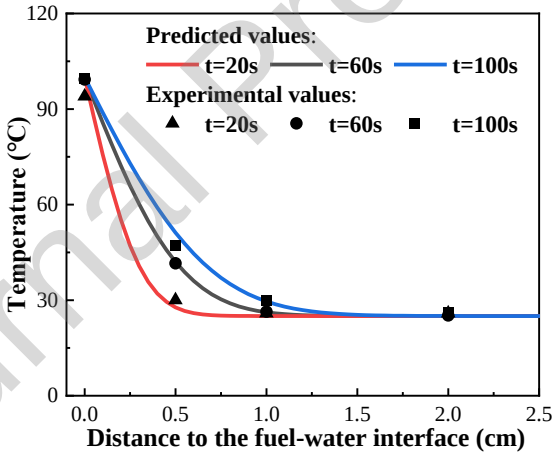

Fig. 11. Comparison between the experimental temperatures at different times and the predicted values for the thermocouple tree positioned 20 cm to the outlet in Test 8.

Figure 12 shows the schematic diagram of the spread process and the heat loss of the fuel layer for a given time ($t = t'$).

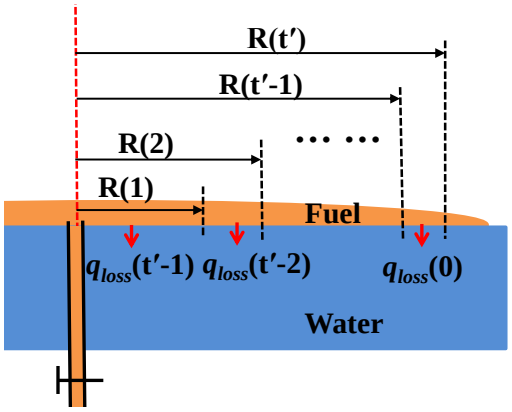

Fig. 12. Schematic diagram of the spread process and heat loss distribution for burning fuel layer (t= t').

In Fig 12, the initial spread radius $R(1)$ was calculated by Eq. (3), and the burning rate at the first time step was assumed to be zero. The total heat loss at the time of t' (R= R (t')) can be calculated as:

$$q'_{loss}(t') = \frac{\sum_{t=1}^{t'} q_{loss}(t\prime-t)\left[\pi R(t)^2-\pi R(t-1)^2\right]}{\pi R(t\prime)^2}, \quad (t' > 1s) \tag{28}$$

From the radiative heat feedback from the flame and the heat loss of the fuel layer, the coefficient C_δ can be obtained. Combined with Eq. (14), the burning rate at the time of t' can thus be derived. Finally, the total fuel volume used for the spread can be found as:

$$Q_{eff} = Q_{in} - \pi\omega_{spill}R(t')^2 \tag{29}$$

Note that in the present calculations the variation of some fuel properties, such as viscosity, and surface tension, were not considered because the spread was mainly controlled by the gravity-inertia regime. Based on Eqs. (2-3, 14 and 28), the maximum spread burning area can be estimated, as shown in Fig. 13.

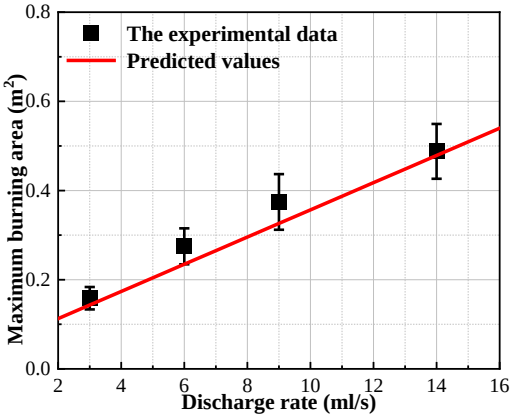

Fig. 13. Comparison of the predicted and measured maximum burning area.

In Fig. 13, the predictions follow the trends of the experimental data and are also in

quantitative agreement with a maximum difference less than 14.5%. The predicted values are slightly lower than the experimental values for some cases, which indicates that the radiative heat feedback could be over-predicted. In addition, the fresh supplied fuel could also affect the heat transfer process. Both factors would result in a lower burning rate and consequently a larger maximum burning area as shown by the experiment data.

4. Conclusion

This study aims to examine the spread and burning behaviors of continuous spill fires on a water surface. A series of large-scale spill fire experiments was performed with different fuel discharge rates and ignition delays. The main conclusions are:

(1) The spread process for the continuous spill can be well predicted using the existing spread model by Briscoe and Shaw as: $R = \left[\frac{4}{3}\varepsilon\left(\frac{1}{\pi}\right)^{1/2}\right]^{1/2}(g'Q_{in})^{1/4}t^{3/4}$, where the spread coefficient ε is found to be 0.23 in this work. Both the maximum and quasi-steady burning areas increase with the discharge rate. The quasi-steady burning area is independent of the ignition delay whereas the maximum burning area increases with increasing ignition delay.

(2) The burning rate of spill fires at the quasi-steady stage is lower than that of pool fires of the same burning area, (from 45 to 62 %). The increased heat loss of the fuel layer to the water layer is the primary reason. The heat loss was incorporate into a theoretical model for calculating the quasi-steady burning rate of a spill fire.

(3) For the quasi-steady flame height, the values predicted by the Heskestad's model proposed for pool fires are slightly lower than the experimental data, likely because of the presence of the side wall in pool fires. Based on the dimensionless analysis and experimental data, a correlation ($H/D = 3.27(\dot{Q}^*)^{0.28}$) was found for continuous spill fires.

(4) Based on the temperature profiles at different depths in the water layer, a simplified one-dimensional conduction model was developed to calculate the heat loss of the fuel layer, which was in turn used in estimating the transient burning rate for the spread burning phase. Combining the spread model and the burning rate model, the maximum burning areas for the spill fires with different discharge rates were predicted and validated against the experimental data.

This study provides a detailed analysis of the spread and burning process for continuous spill fires on a water surface. The experimental data (especially the burning

rate and the maximum burning area) and the developed correlations and models are not only useful in explaining the differences between the burning of spill fires and pool fires, but of practical importance in understanding and assessing the risks associated with marine transportation of liquid fuels, and the subsequent risk management and mitigation (e.g., the use of in-situ burning).

Acknowledgements

This study was sponsored by the National Natural Science Foundation of China (No. 51906253 and No. 51806247), the Fundamental Research Funds for the Central Universities (No. 2020QN05 and No. 2021JCCXAQ01).

References

Babrauskas, V., 1983. Estimating large pool fire burning rates. Fire Technol. 19, 251-261.

Bonvicini, S., Antonioni, G., Morra, P., Cozzani, V., 2015. Quantitative assessment of environmental risk due to accidental spills from onshore pipelines. Process Saf. Environ. Protect. 93, 31-49.

Brambilla, S., Manca, D., 2009. Accidents involving liquids: a step ahead in modeling pool spreading, evaporation and burning. J. Hazard. Mater. 161, 1265-1280.

Briscoe, F., Shaw, P., 1980. Spread and evaporation of liquid. Prog. Energy Combust. Sci. 6, 127-140.

Ditch, B.D., de Ris, J.L., Blanchat, T.K., Chaos, M., Bill Jr, R.G., Dorofeev, S.B., 2013. Pool fires–An empirical correlation. Combust. Flame 160, 2964-2974.

Fay, J.A., 1969. The spread of oil slicks on a calm sea, Oil on the Sea. Springer, pp. 53-63.

Fay, J.A., 2003. Model of spills and fires from LNG and oil tankers. J. Hazard. Mater. 96, 171-188.

Garo, J., Gillard, P., Vantelon, J., Fernandez-Pello, A., 1999. Combustion of liquid fuels spilled on water. Prediction of time to start of boilover. Combust. Sci. Technol. 147, 39-59.

Gottuk, D., Scheffey, J., Williams, F., Gott, J., Tabet, R., 2000. Optical fire detection (OFD) for military aircraft hangars: final report on OFD performance to fuel spill fires and optical stresses. Naval Research Laboratory, Washington.

Hamins, A., Fischer, S., Kashiwagi, T., Klassen, M., Gore, J., 1994. Heat feedback to the fuel surface in pool fires. Combust. Sci. Technol. 97, 37-62.

Heskestad, G., 1999. Turbulent jet diffusion flames: consolidation of flame height data. Combust. Flame 118, 51-60.

Ingason, H., Li, Y.Z., 2017. Spilled liquid fires in tunnels. Fire Saf. J. 91, 399-406.

Lehr, W., Simecek-Beatty, D., 2004. Comparison of hypothetical LNG and fuel oil fires on water. J. Hazard. Mater. 107, 3-9.

Li, H., Liu, H., Liu, J., Ge, J., Tang, F., 2021a. Spread and burning characteristics of continuous spill fires in a tunnel. Tunn. Undergr. Space Technol. 109.

Li, H., Liu, J., Ge, J., 2020. Phenomenological characteristics of continuous spill fires in a tunnel with longitudinal ventilation. Process Saf. Environ. Protect. 138, 108-116.

Li, Y., Huang, H., Zhang, L., Su, B., Zhao, J., Liu, Q., 2017. An experimental investigation into the effect of substrate slope on the continuously released liquid fuel spill fires. J. Loss Prev. Process Ind. 45, 203-209.
Mealy, C., Benfer, M., Gottuk, D., 2014. Liquid Fuel Spill Fire Dynamics. Fire Technol. 50, 419-436.
Moorhouse, J., 1982. Scaling criteria for pool fires derived from large scale experiments.
Palazzi, E., Currò, F., Fabiano, B., 2004. Simplified Modelling for Risk Assessment of Hydrocarbon Spills in Port Area. Process Saf. Environ. Protect. 82, 412-420.
Pan, Y., Li, M., Luo, X., Wang, C., Luo, Q., Li, J., 2020. Analysis of heat transfer of spilling fire spread over steady flow of n-butanol fuel. Int. Commun. Heat Mass Transf. 116.
Raj, P.K., 2011. Evaporating liquid flow in a channel (An integral model based on shallow water flow approximation). J. Loss Prev. Process Ind. 24, 886-899.
Raja, S., Abbasi, T., Tauseef, S.M., Abbasi, S.A., 2019. Equilibrium models for predicting areas covered by accidentally spilled liquid fuels and an assessment of their efficacy. Process Saf. Environ. Protect. 130, 153-162.
Soares da Silva, R.d.C.F., Luna, J.M., Rufino, R.D., Sarubbo, L.A., 2021. Ecotoxicity of the formulated biosurfactant from Pseudomonas cepacia CCT 6659 and application in the bioremediation of terrestrial and aquatic environments impacted by oil spills. Process Saf. Environ. Protect. 154, 338-347.
Suo-Anttila, J.M., Blanchat, T.K., Ricks, A.J., Brown, A.L., 2009. Characterization of thermal radiation spectra in 2 m pool fires. Proc. Combust. Inst. 32, 2567-2574.
Vali, A., Nobes, D.S., Kostiuk, L.W., 2015. Fluid motion and energy transfer within burning liquid fuel pools of various thicknesses. Combust. Flame 162, 1477-1488.
Webber, D., 2012. On models of spreading pools. J. Loss Prev. Process Ind. 25, 923-926.
Yin, F., Song, Z., Wei, Q., Zhao, X., Su, P., Huang, H., 2021. Characterization of polycyclic aromatic hydrocarbons in the surface sediments around the sunken Sanchi oil tanker. Mar. Pollut. Bull. 164, 112098.
Zhao, J., Huang, H., Li, Y., Jomaas, G., Wang, H., Zhong, M., 2017. Quantitative risk assessment of continuous liquid spill fires based on spread and burning behaviours. Appl. Therm. Eng. 126, 500-506.
Zhao, J., Zhang, J., Chen, C., Huang, H., Yang, R., 2020. Experimental investigation on the burning behaviors of thin-layer transformer oil on a water layer. Process Saf. Environ. Protect. 139, 89-97.
Zhao, J., Zhu, H., Huang, H., Zhong, M., Yang, R., 2019. Experimental study on the liquid layer spread and burning behaviors of continuous heptane spill fires. Process Saf. Environ. Protect. 122, 320-327.
Zukoski, E.E., Cetegen, B.M., Kubota, T., 1985. Visible structure of buoyant diffusion flames. Symp. Combust. 20, 361-366.

Declaration of Competing Interest

The authors declare that they have no known competing financial interests or personal relationships that could have appeared to influence the work reported in this paper.